Accepted Manuscript

Sterically Induced Conformational Restriction: Discovery and Preclinical Evaluation of Novel Pyrrolo[3, 2-*d*]pyrimidines as Microtubule Targeting Agents

Roheeth Kumar Pavana, Khushbu Shah, Taylor Gentile, Nicholas F. Dybdal-Hargreaves, April L. Risinger, Susan L. Mooberry, Ernest Hamel, Aleem Gangjee

PII: S0968-0896(18)31327-0
DOI: https://doi.org/10.1016/j.bmc.2018.09.025
Reference: BMC 14550

To appear in: *Bioorganic & Medicinal Chemistry*

Received Date: 23 July 2018
Revised Date: 11 September 2018
Accepted Date: 20 September 2018

Please cite this article as: Pavana, R.K., Shah, K., Gentile, T., Dybdal-Hargreaves, N.F., Risinger, A.L., Mooberry, S.L., Hamel, E., Gangjee, A., Sterically Induced Conformational Restriction: Discovery and Preclinical Evaluation of Novel Pyrrolo[3, 2-*d*]pyrimidines as Microtubule Targeting Agents, *Bioorganic & Medicinal Chemistry* (2018), doi: https://doi.org/10.1016/j.bmc.2018.09.025

Sterically Induced Conformational Restriction: Discovery and Preclinical Evaluation of Novel Pyrrolo[3, 2-*d*]pyrimidines as Microtubule Targeting Agents

Roheeth Kumar Pavana,[a] Khushbu Shah,[a] Taylor Gentile,[a] Nicholas F. Dybdal-Hargreaves,[b] April L. Risinger,[b] Susan L Mooberry,[b,#] Ernest Hamel,[c] Aleem Gangjee[a,*,#]

[a]Division of Medicinal Chemistry, Graduate School of Pharmaceutical Sciences, Duquesne University, Pittsburgh, PA 15282, **gangjee@duq.edu**, Fax: 412-396-5593

[b]Department of Pharmacology, Cancer Therapy & Research Center, University of Texas Health Science Center at San Antonio, 7703 Floyd Curl Drive, San Antonio, TX 78229

[c]Screening Technologies Branch, Developmental Therapeutics Program, Division of Cancer Treatment and Diagnosis, National Cancer Institute at Frederick, National Institutes of Health, Frederick, Maryland 21702, United States

[#]These authors contributed equally to this work.

Abbreviations: MTA, microtubule targeting agents; Pgp, P-glycoprotein; CA-4, combretastatin A-4

Abstract

The discovery, synthesis and biological evaluations of a series of nine N5-substituted-pyrrolo[3,2-*d*]pyrimidin-4-amines are reported. Novel compounds with microtubule depolymerizing activity were identified. Some of these compounds also circumvent clinically relevant tumor resistance mechanisms (expression of P-glycoprotein and βIII tubulin). Compounds **4**, **5**, and **8-13** were one to two-digit nanomolar (IC_{50}) inhibitors of cancer cells in culture. Contrary to recent reports (Banerjee et al. *J. Med. Chem.* **2018**, *61*, 1704-1718), the conformation of the most active compounds determined by ^{1}H NMR and molecular modeling are similar to that reported previously and in keeping with recently reported x-ray crystal structures. Compound **11**, freely water soluble as the HCl salt, afforded statistically significant inhibition of tumor growth in three xenograft models [MDA-MB-435, MDA-MB-231 and NCI/ADR-RES] compared with controls. Compound **11** did not display overt animal toxicity and is currently slated for further preclinical development.

Keywords

microtubule depolymerizers, microtubule targeting agents, pyrrolo[3, 2-*d*]pyrimidines, preclinical agents, P-glycoprotein, βIII tubulin

1. Introduction

Aberrant, chronic proliferative signaling is one of the six major hallmarks of cancer.[1] Microtubules have multiple roles during all phases of the cell cycle that facilitate oncogenic cellular proliferation. While the roles of microtubules in mitosis are well documented, they are also critical for intracellular transport, maintenance of cell shape and polarity, activation of immune cells, and cellular signaling. These events, in addition to mitosis, are inhibited by the actions of microtubule targeting agents (MTAs).[2-4] MTAs produce their effects by suppressing microtubule dynamics leading to stabilization or depolymerization of the cellular microtubule network.[5] MTAs are among the most clinically successful anticancer agents and are of significant importance as the only class of cytotoxic agents effective against the 39 cancer cell lines with p53 mutations in the NCI 60-cell line panel.[6, 7]

We previously reported the identification of substituted pyrrolo[3,2-*d*]pyrimidines, compounds **1-4** (Fig. 1) that are water-soluble colchicine site microtubule depolymerizing agents.[8] In this study, we report structural modifications of these compounds that led to significant improvement in their potency as MTAs. These analogs also circumvent drug resistance mechanisms, including expression of P-glycoprotein (Pgp) and βIII tubulin, which limit the clinical utility of MTAs.

2. Rationale

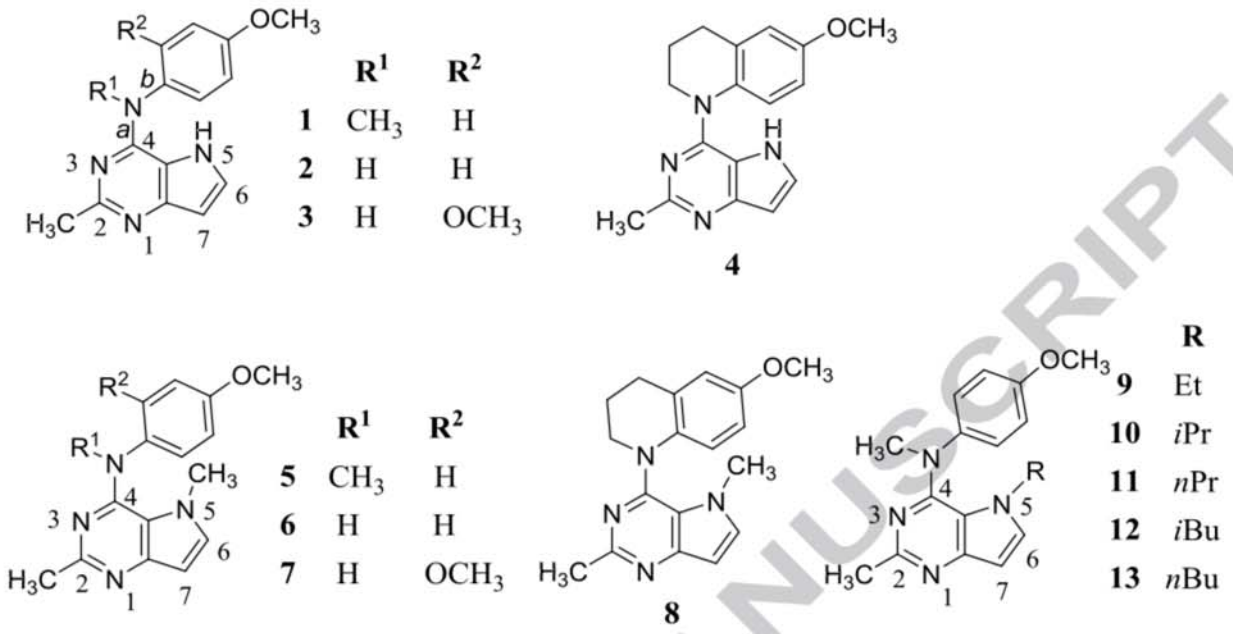

Figure 1. Structures of compounds **1-13**

We previously reported the synthesis and biological activities of compounds **1-4** (Fig. 1) that contain the pyrrolo[3,2-*d*]pyrimidine scaffold.[8] Compounds **1** and **4** were identified as water-soluble, colchicine site binding MTAs.[8] Conformational restriction of bond b in **1** by its incorporation into a ring afforded **4**, with greater than two-fold increased potency against cancer cells compared to **1** (Table 1). To identify a potential clinical lead candidate, structural modifications of **1** and **4** were carried out which led to the design of additional conformationally restricted analogs. Compound **5** contains a N5-CH_3 that restricts the rotation of both bonds a and b (designated in Fig. 1). Low energy conformations of the proposed compounds were generated using Sybyl-X 2.1,[9] and the number of conformations within 1 kcal/mol obtained for **1** and **5** were 88 and 53, respectively. Thus, **5**, the N5-CH_3 analog of **1**, displays a lower number of conformations due to conformational restriction across bonds a and b. In previous studies, we

discovered that the methyl group on the N4 is essential for potent activity as a MTA.[8, 10, 11] Compounds **6** and **7** with a N5-CH_3 moiety were designed to restrict conformation about bonds a and b in the absence of the N4-CH_3, in an attempt to determine if the N5-CH_3 could sterically mimic the functions of the N4-CH_3 and compensate for its absence and its conformational influence on bonds a and b. The number of low energy conformations of **6** and **7** within 1 kcal/mol were found to be 87 and 65, respectively, suggesting a restricted conformation, compared to **1** (88 low energy conformations), at least for **7**. In compound **7** an additional 2'-OCH_3 was incorporated to ascertain if this would facilitate greater potency by mimicking the ketone of the C-ring of colchicine. Compound **4**, the 1,2,3,4-tetrahydroquinoline derivative, which is a conformationally restricted analog of **1**, is 5-fold more potent[8] in the microtubule depolymerization assay and more than twice as potent against cancer cells than **1** (Table 1). The N5-CH_3 moiety of **8** could provide further conformational rigidity compared to **4**, which we hypothesized could increase potency.

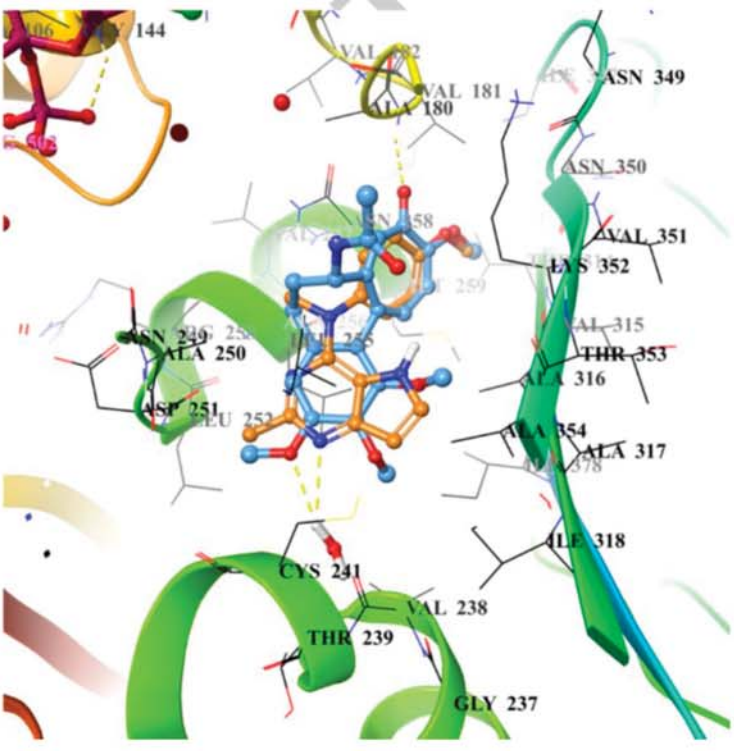

A

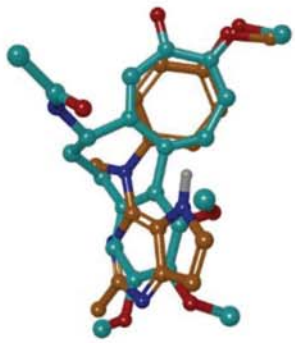

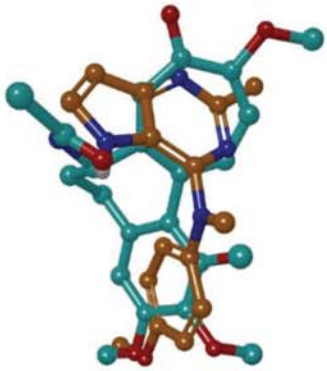

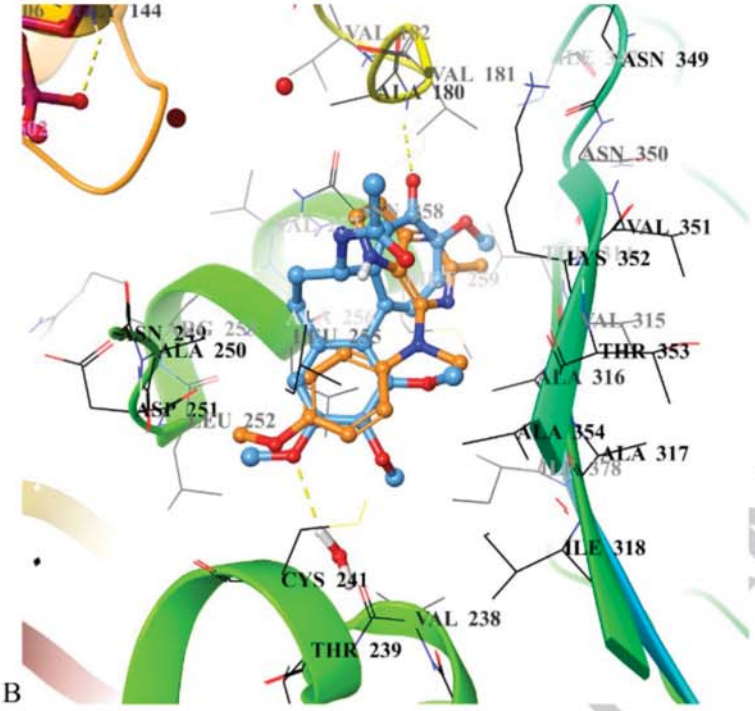

B

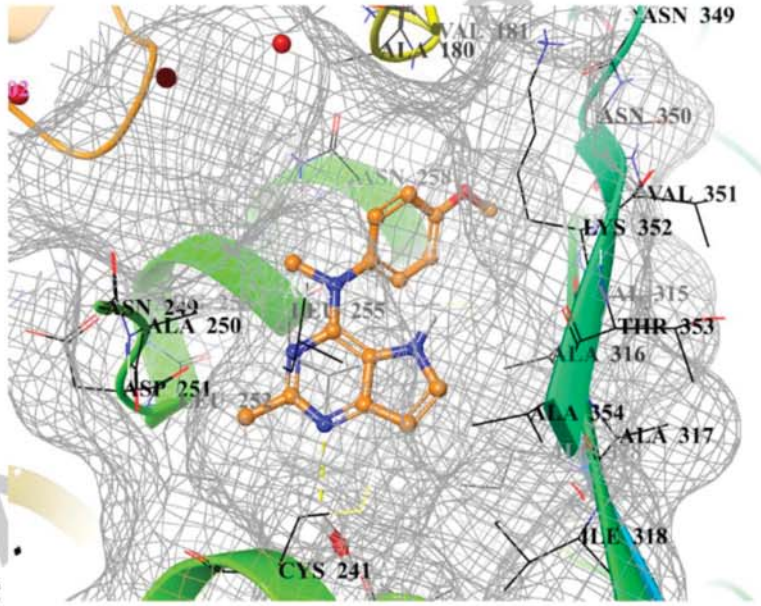

C

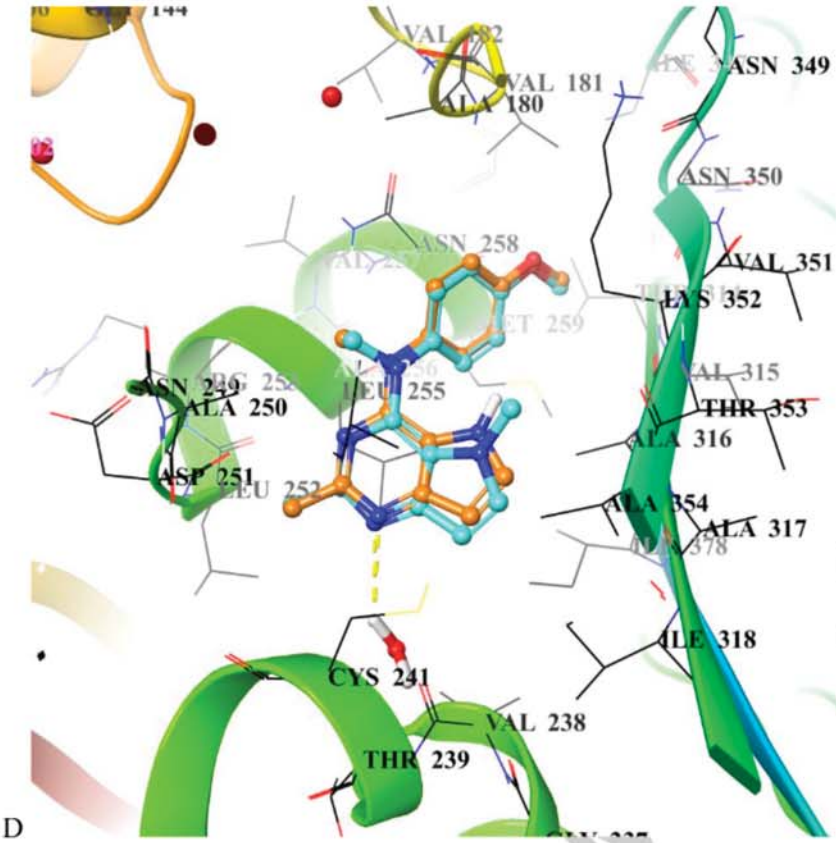

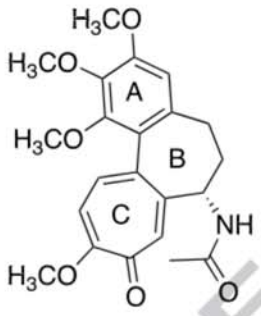

Colchicine

Figure 2. A) Superimposition of the best docked pose of **1** (tan carbons) and colchicine (cyan carbons) in tubulin (PDB ID: 4O2B)[12] with extracted posed ligands on the right. B) Superimposition of an alternate pose of **1** (tan carbons) and colchicine (cyan carbons) in tubulin (PDB ID: 4O2B)[12] with extracted posed ligands on the right. C) Binding site surface of the colchicine site on tubulin. D) Superimposition of docked pose of **5** (cyan carbons) and **1** (tan

carbons) in tubulin (PDB ID: 4O2B).[12] The grey and black polypeptide chains represent α- and β-tubulin, respectively.

To support our design and structural modifications, we carried out molecular modeling studies using Schrödinger.[13] Compounds **1-13** were docked in the X-ray crystal structure of the colchicine site of tubulin (PDB: 4O2B, 2.3 Å),[12] using the parameters specified in the experimental section. Multiple low energy conformations with distinct bonding modes were obtained on docking. As a representative example, Fig. 2A shows one of the docked conformations of **1** (tan carbons) superimposed on the co-crystallized ligand, colchicine (cyan carbons). The pyrrolo[3,2-*d*]pyrimidine scaffold of **1** forms hydrophobic interactions with Leuα252, Alaα316, Leuβ248, Alaβ250, and Leuβ255 and occupies the region where the A-ring of colchicine binds. The N1 of the pyrrolo[3,2-*d*]pyrimidine scaffold of **1** forms hydrogen bond with a water molecule in the crystal structure bonded to Valβ238 and Cysβ241. The N4-CH_3 interacts with Leuβ255 through hydrophobic interactions. The p-methoxyaniline ring of **1** occupies the region where the C-ring of colchicine binds, forming hydrophobic interactions with Thrα314, Valα351, Alaα316, and Alaβ180.The best-docked pose of **1** had a score of -6.83 kcal/mol.

Another distinct pose of **1** was also obtained through molecular modeling, as depicted in Fig. 2B. In this particular pose the pyrrolo[3,2-*d*]pyrimidine scaffold of **1** forms hydrophobic interactions with Alaα180, Valα181, and Metβ259 and occupies the region where the C-ring of colchicine binds. The N4-CH_3 interacts with Alaβ316 through hydrophobic interactions. The *p*-methoxyaniline ring of **1** occupies the region where the A-ring of colchicine binds, forming hydrophobic interactions with Leuα252, Alaα316, Leuβ248, Alaβ250, and Leuβ255. The oxygen

atom of the 4'-OCH_3 group of **1** lies within H-bonding distance of a water molecule in the crystal structure, in the vicinity of Cysβ241. This docked pose of **1** had a score of -6.09 kcal/mol. Since both poses for **1** are within 1 kcal/mol, the reference pose represented in Fig. 2A was chosen based on the X-ray crystal structure (PDB ID: 6BR1)[14] of a structurally similar pyrimidine-fused compound (quinazoline analog) that binds to the colchicine site of tubulin. Studying the colchicine binding site of **1** (Fig. 2C) suggests that the N5-H of **1** is oriented towards a hydrophobic pocket created in the vicinity of Valβ315 and Alaβ316. This suggests that alkyl substituents at this position can facilitate better binding to the active site of tubulin**.** Fig. 2D displays the best-docked pose of **5** (cyan carbons) superimposed on the best-docked pose of **1** (tan carbons). The mode of binding of **5** was similar to that of compound **1,** with a docked score of -7.23 kcal/mol. Compounds **9-13** extend the N5-alkyl substitution of **5** with larger alkyl groups to determine the size of the hydrophobic pocket. The docked score for **7** was -7.79 kcal/mol. All the proposed compounds **6-13** displayed docked poses similar to that of compound **5**, with docked scores in the range of -5.86 to -7.41 kcal/mol. These scores suggest that the designed analogs **5-13** should afford equal or better microtubule targeting activity than **1**.

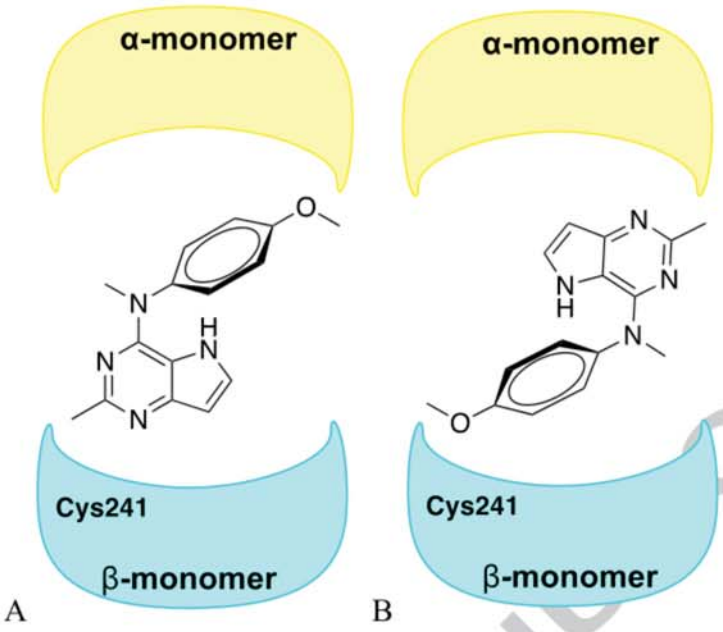

Figure 3. A) Diagrammatic representation of the best binding pose for **1** in tubulin (PDB ID: 4O2B)[12] and B) Diagrammatic representation of the second-best binding pose for **1** in tubulin (PDB ID: 4O2B).[12]

Cartoons of representative poses for the compounds are shown in Fig. 3. Despite obtaining two flipped poses about the monomers of tubulin, both the molecular modeling poses for each of the compounds had a specific orientation of the 4-methoxyphenyl or 6-methoxyquinoline relative to the pyrrolo[3,2-*d*]pyrimidine scaffold – the phenyl ring is oriented on top of the 5-N of the pyrrole ring (as illustrated in Fig. 2A/3A and 2B/3B). The orientation of the phenyl ring relative to the pyrimidine fused heterocycle shown in Fig. 2B and 3B and in previously reports[11, 15] are distinct from the modeling reported by Banerjee *et al.*[14] that show a 180-degree rotation of the C4-N bond . The importance and designation of the orientation for the phenyl ring has been previously described in detail.[11] Poses similar to 2A/3A and 2B/3B were revealed from the molecular modeling of **8**. In keeping with the recently reported crystal

structure[14] and the molecular modeling of **1** and **5**, the pose with the phenyl ring oriented on top of the 5-N of the pyrrole ring was also obtained for **8**.

3. Chemistry

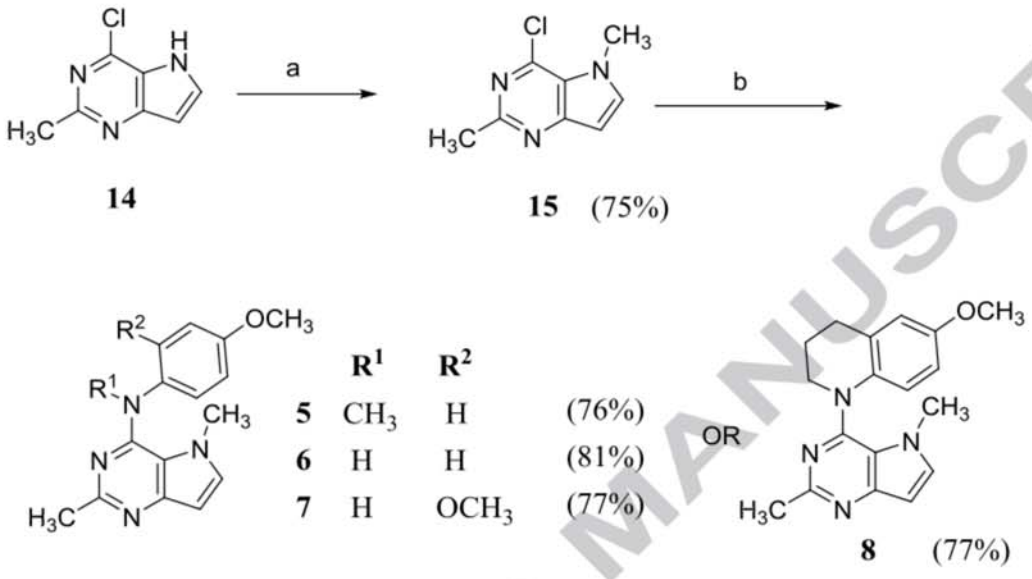

Scheme 1. Reagents and conditions: (a) NaH, CH_3Br, DMF (b) appropriately substituted amine, isopropanol, reflux, 4-24 h

The key intermediate 4-chloro-2-methyl-5*H*-pyrrolo[3,2-*d*]pyrimidine **14** (Scheme 1) was synthesized as previously described.[8] Compound **14** was deprotonated with sodium hydride and methylated using methyl bromide to afford **15**, which, on treatment with appropriately substituted amines in isopropanol at reflux, afforded compounds **5**-**8**.

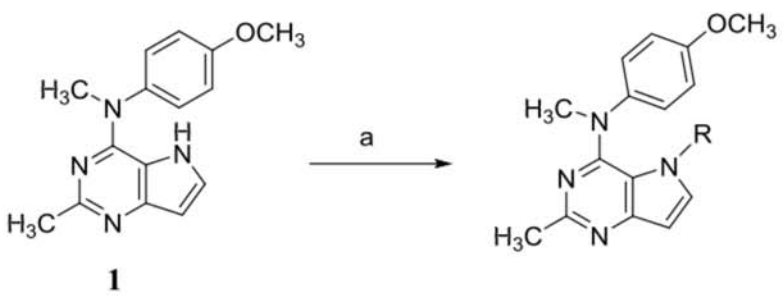

	R	
9	Et	(75%)
10	*i*Pr	(78%)
11	*n*Pr	(83%)
12	*i*Bu	(80%)
13	*n*Bu	(77%)

Scheme 2. Reagents and conditions: (a) NaH, alkyl halide, DMF, 2-8 h

Pyrrolo[3,2-*d*]pyrimidine **1** (Scheme 2),[8] was deprotonated with sodium hydride and treated with the appropriate alkyl halide to afford the corresponding *N5*-alkylated pyrrolo[3,2-*d*]pyrimidines **9-13**. Reactions involving combinations of cesium carbonate or potassium carbonate and dimethylformamide with microwave irradiation or conventional bench-top conditions did not show complete consumption of starting material by TLC. In addition, the mixture of **1** and the alkylated product could not be separated by column chromatography. The use of excess base or alkyl halide did not afford the desired alkylated product exclusively. To overcome these problems, the deprotonation-alkylation sequence described in Scheme 2 was chosen as the method for alkylation of **1** to **9-13**.

4. Biological evaluations and discussion

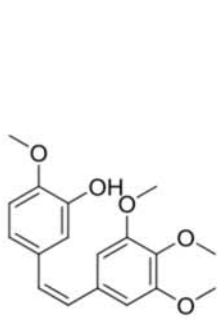

Combretastatin A-4

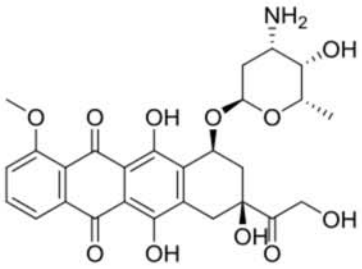

Doxorubicin

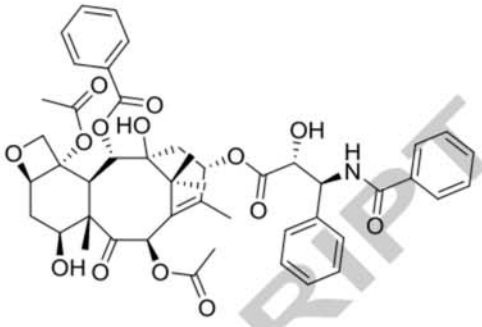

Paclitaxel

Figure 4. Standards used in biological assays

4.1 Microtubule depolymerization, colchicine binding and anti-proliferative effects

Table 1: Microtubule depolymerization activity, inhibition of [^{3}H]colchicine binding, and antiproliferative effects.

	Microtubule depolymerization EC_{50} (nM)	Antiproliferative effects	Inhibition of [^{3}H]colchicine binding % inhibition ± SD	
		MDA-MB-435 IC_{50} (nM) ± SD	5 μM inhibitor	0.5 μM inhibitor
1·HCl[8]	1200	96 ± 5	60 ± 1	ND
2·HCl[8]	> 10,000	ND	5.8 ± 0.9	ND
3·HCl[8]	> 10,000	ND	0	ND
4·HCl[8]	230	43 ± 3	70 ± 5	ND
5·HCl	7.4	4.3 ± 0.3	99 ± 2	79 ± 0.8
6·HCl	> 10,000	ND	4.2 ± 5	ND
7·HCl	> 10,000	ND	14 ± 5	ND
8·HCl	39	21 ± 4	98 ± 0.3	72 ± 4
9	28	10.8 ± 0.3	96 ± 1	79 ± 2
10·HCl	42	21 ± 2	92 ± 0.06	60 ± 4
11·HCl	20	9 ± 3	97 ± 0.1	86 ± 2
12·HCl	55	39 ± 5	95 ± 0.3	67 ± 3
13·HCl	32	27 ± 4	96 ± 1	82± 3
CA-4	9.8	4.4 ± 0.5	99 ± 0.7	86 ± 3

ND: not determined

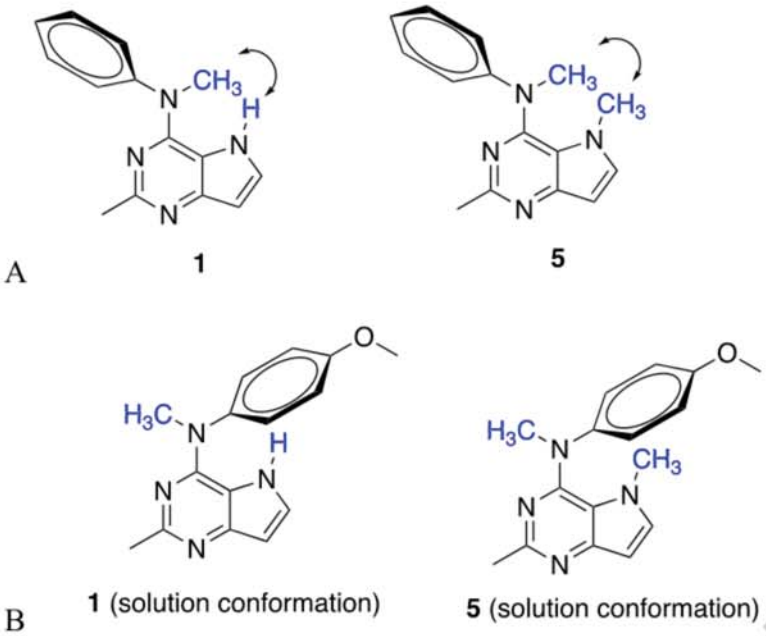

Figure 5. A) Representation of possible steric hindrance between N4-CH_3 and H and CH_3 in **1** and **5,** respectively and B) The conformation as predicted from the ^{1}H NMR proton shifts.

Microtubule depolymerization activities: Compounds **5-13** were evaluated for their ability to disrupt cellular microtubules, and their activities were compared with that of combretastatin A-4[16] (CA-4, Fig. 4). EC_{50} values (the concentration that causes loss of 50% of cellular microtubules in A-10 cells) were determined only for compounds that caused at least 50% microtubule depolymerization at 10 μM. A-10 cells facilitate quantification of effects on interphase microtubules because, unlike cancer cells, they do not accumulate in mitosis following treatment with MTAs. Compound **5**, the N5-CH_3 analog of **1**, was the most potent inhibitor of microtubule depolymerization in this series, with potency similar to that of CA-4. It was over 150-fold more potent than **1**, indicating that N5-methylation of the pyrrolo[3,2-*d*]pyrimidine is required for potent microtubule depolymerizing activity. The improvement in the microtubule depolymerization activity of **5** can be explained by studying the stable solution

conformations of **1** and **5** using ^{1}H NMR. The N4-CH_3 causes the phenyl ring to be oriented in such a manner that the 5-NH falls inside the anisotropic cone of the phenyl ring, as observed from the ^{1}H NMRs of **1** and **2**.[8] A similar effect is seen on the 5-CH_3 of **5**. On comparing the chemical shifts of 5-CH_3 in **5** (2.83 ppm) vs. **6** (4.23 ppm), a shielding of over 1 ppm is observed for the 5-CH_3 in **5**. The 4-methoxyphenyl group causes an anisotropic effect on 5-H and 5-CH_3 of **1** and **5**, respectively (Fig. 5). This solution conformation of **1** is possibly due to steric hindrance between the 5-H and the N4-CH_3, which is further reinforced in **5** by steric hindrance between the 5-CH_3 and the N4-CH_3 (Fig. 5). Similarly, compound **8**, the N5-methyl analog of **4**, was 6-fold more potent than **4** with regard to microtubule depolymerization. The effects of conformational restriction using a tetrahydroquinoline (**1** vs **4**) and using N5-methylation (**1** vs **5)** were not additive (**4** vs **8**). The 4-NH analogs **6** and **7** showed less than 50% inhibition of microtubule depolymerization at 10 μM. The additional 2'-OCH_3 moiety incorporated in **7** to mimic the C-ring of colchicine did not improve activity compared to **6,** thus suggesting that N5-methylation alone is not sufficient to significantly improve the microtubule depolymerizing activities of **6** and **7** in comparison with **2** and **3**, reiterating the importance of the N4 methyl group for inhibition of tubulin polymerization.[8, 10, 11] Compounds **9-13** were about 20- to 60- fold more potent than **1** for microtubule depolymerizing activity, but less potent than **5** in this assay. The N5-alkyl groups can have two effects: allowing additional hydrophobic interactions with tubulin and/or restricting the rotation around the N-phenyl bond due to steric bulk, thus providing conformational rigidity. This slight decrease in potency of compounds **9-13**, compared to **5** could be due to additional bulk at N5-position in **9-13**, which can affect the orientation of the 4-methoxyphenyl group of these compounds thus causing a slight deviation between the stable solution conformation and the binding conformation.

Compounds **5** and **8-13**, which showed potent microtubule depolymerizing activities, strongly inhibited [^{3}H]colchicine binding with percent inhibition values comparable to CA-4, indicating that they are colchicine site MTAs (Table 1).

4.2 Effects of βIII-tubulin or Pgp overexpression on antiproliferative potency

Table 2: Inhibition of growth of βIII-tubulin or Pgp expressing cells

	IC_{50} ± SD in HeLa (nM)	IC_{50} ± SD in HeLa WTβIII (nM)	Rr Value	IC_{50} ± SD in SK-OV-3 (nM)	IC_{50} ± SD in SK-OV-3 MDRI-M6/6 (nM)	Rr Value
5·HCl	5.0 ± 0.3	4.3 ± 0.2	0.9	5.2 ± 0.4	6 ± 2	1.2
8·HCl	27 ± 2	33 ± 2	1.2	30 ± 2	31.5 ± 0.3	1.1
9	17 ± 3	14 ± 3	0.8	17 ± 2	19.3 ± 0.9	1.1
10·HCl	32 ± 3	20 ± 2	0.6	31 ± 3	58 ± 3	1.9
11·HCl	5.9 ± 0.4	5.1 ± 0.7	0.9	5 ± 1	7± 1	1.4
12·HCl	26 ± 3	23 ± 6	0.9	26 ± 4	25 ± 10	1.0
13·HCl	14 ± 2	10 ± 2	0.7	13 ± 1	15 ± 4	1.2
CA-4	3.3 ± 0.4	3.3 ± 0.3	1.0	5.5 ± 0.5	7 ± 1	1.3
Paclitaxel	2.8 ± 0.4	24 ± 3	8.6	5.0 ± 0.6	1200 ± 60	240

The ability of MTAs **5** and **8-13** to overcome drug resistance mediated by βIII-tubulin or Pgp was evaluated with two isogenic cell line pairs (Table 2). The ability of compounds to overcome resistance is represented by the relative resistance (Rr) value. The Rr value is obtained by dividing IC_{50} values obtained in the resistant cells by IC_{50} obtained in the parental cells. A low Rr indicates that the parental and resistant cell lines have similar sensitivity to the compound and high Rr value indicates poor sensitivity of the resistant cells to the compound. Paclitaxel had

an Rr value of 8.6 in the βIII-tubulin expressing cell line as compared to the parental HeLa cell line. These two cell lines were equally sensitive to **5** and **8-13** with Rr values of 0.6 – 1.2, demonstrating that, like the CA-4 control, these compounds can circumvent βIII-tubulin-mediated drug resistance. Compounds **5** and **8-13** were also evaluated in the isogenic SK-OV-3 and SK-OV-3 MDRI-M6/6 cell line pair to determine their susceptibility to Pgp-mediated drug resistance (Table 2). The Rr value of paclitaxel in this cell line pair is 240, consistent with the fact that paclitaxel is a known Pgp substrate. The Rr values of compounds **5** and **8-13** were each less than 2, suggesting that they are poor substrates for Pgp-mediated transport and are able to overcome drug resistance mediated by Pgp. Hence, compounds **5** and **8-13** are not susceptible to either Pgp or βIII-tubulin mediated drug resistance mechanisms that can limit the clinical utility of MTAs, including paclitaxel, docetaxel, vinblastine and vinorelbine.

4.3 In vivo efficacy in a MDA-MB-435 xenograft trial

Compounds **5** and **11**, the two most potent compounds in the cytotoxicity and microtubule depolymerization assays (Tables 1 and 2), were selected for in vivo evaluation in xenograft mouse models. MDA-MB-435 tumor fragments were implanted subcutaneously into both flanks of nude mice. Mice were treated using IP injections of 75 mg/kg/dose. (cumulative dose: 375 mg/kg for **5** and 525 mg/kg for **11**) and compared to untreated controls. The results show that both **5** and **11** caused statistically significant inhibition of tumor growth (Fig. 6). In addition, both these compounds caused recoverable weight loss (Fig. 7), however compound **5** also caused noticeable neurological side effects. In contrast, **11** did not induce any noticeable adverse effects or toxicities at this dose other than recoverable weight loss. Therefore, this

compound was selected for evaluation in the more aggressive MDA-MB-231 breast adenocarcinoma xenograft model.

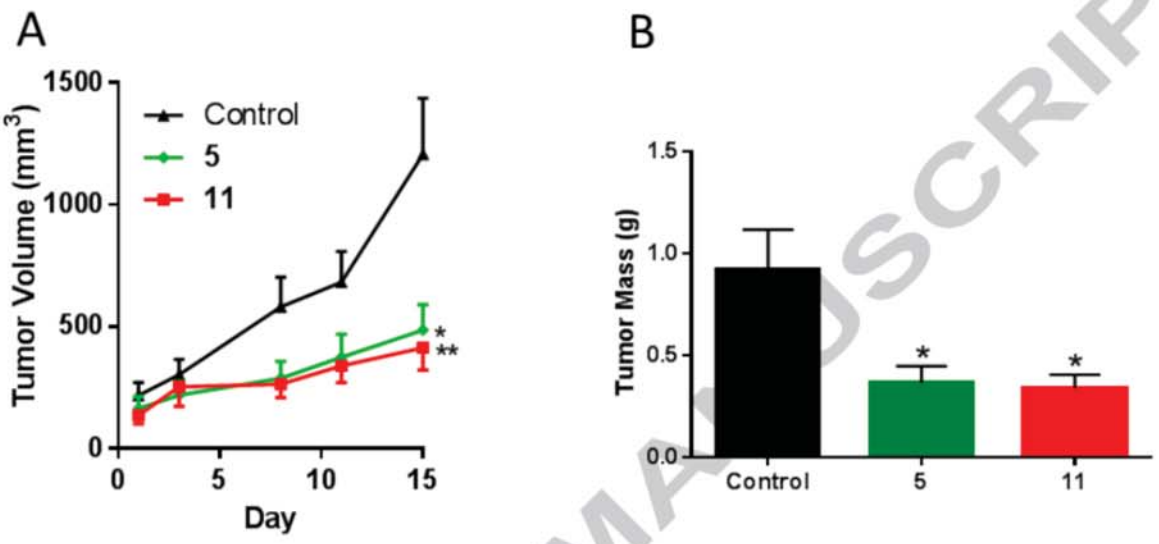

Figure 6. A) Effects of **5** and **11** on growth of MDA-MB-435 tumors.

[Legend]

Compound **5** was administered ip on 5 days (days 1, 2, 3, 4, 9), for a total cumulative dose of 375 mg/kg, and compound **11** was administered on 7 days (1, 2, 3, 4, 7, 9, and 11), for a cumulative dose of 525 mg/kg and compared to untreated controls. n = 10 tumors per group, and data points represent mean tumor volume (mm^3) ± SEM. $^{*}p < 0.05$, $^{**}p < 0.01$ at day 15 as compared with the control. B) Final average mean tumor mass (g) ± SEM on day 15. $^{*}p < 0.05$ as compared with the control.

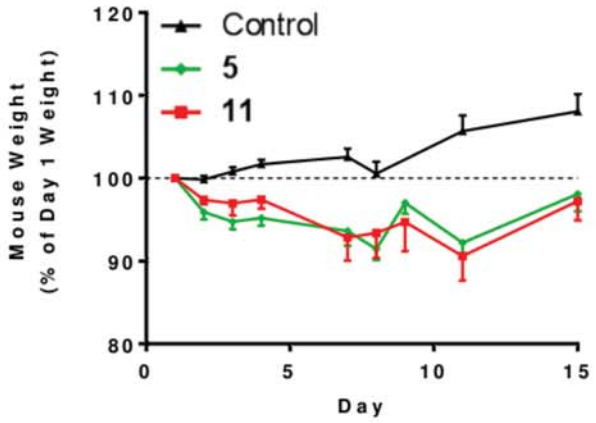

Figure 7. Percent change in mouse weight during treatment with **5** and **11**.

[Legend]

Data points represent mean ± SEM.

4.4 In vivo efficacy in MDA-MB-231 xenograft

The antitumor effects of **11** were evaluated in the MDA-MB-231 xenograft model and compared to paclitaxel. The cumulative dose of paclitaxel was 60 mg/kg and the cumulative dose of **11** was 450 mg/kg. Compound **11** and paclitaxel each caused statistically significant inhibition of increase in tumor volume as compared to control tumors (Fig. 8).

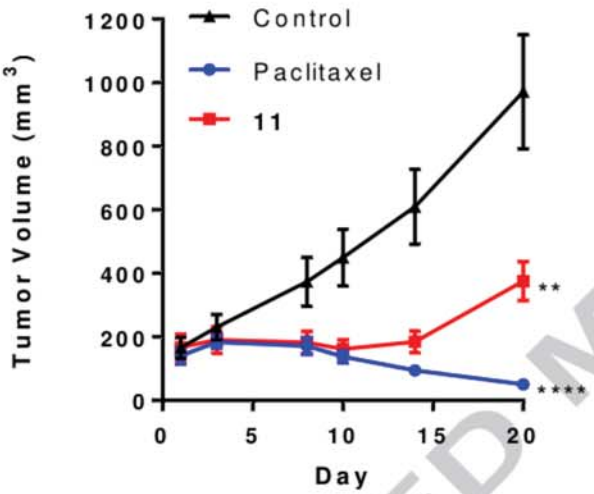

Figure 8. Effects of **11** and paclitaxel on the growth of MDA-MB-231 tumors.

[Legend]

The mean MDA-MB-231 tumor volumes (mm^3) ± SEM over the course of the trial are plotted. Mice were treated with **11** (75 mg/kg) or paclitaxel (10 mg/kg) on days 1, 2, 3, 8, 9 and 10 for cumulative doses of 400 mg/kg for **11** and 60 mg/kg for paclitaxel and compared to control tumors. n = 7-10 tumors per group. The comparisons in tumor volumes between control and drug-treated groups are indicated for day 20. $^{****}p<0.0001$, $^{**}p<0.01$.

4.5 In vivo efficacy in NCI/ADR-RES drug resistant model

Compound **11** was also tested for in vivo antitumor effects in the NCI/ADR-RES model, an aggressive ovarian xenograft model that expresses Pgp (Fig. 9). Mice were treated on days 1, 3, and 5 with 75 mg/kg **11** or 10 mg/kg paclitaxel and compared to untreated controls. On day 9 of the trial the tumor volumes of mice treated with **11** were significantly smaller than those in control mice, while paclitaxel did not cause statistically significant antitumor effects in this drug-resistant model.

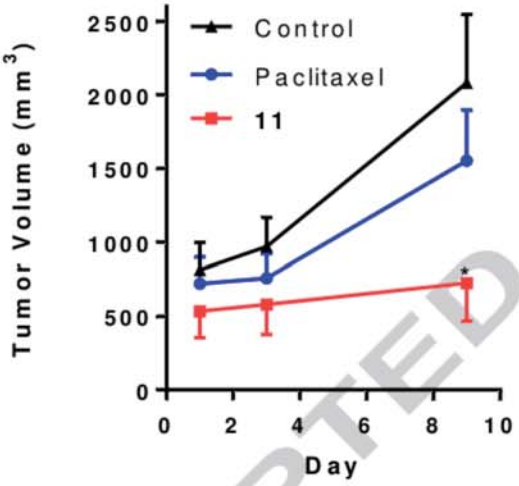

Figure 9. Effects of **11** and paclitaxel on NCI/ADR-RES tumor growth.

[Legend]

The mean tumor volumes ± SEM of mice treated with **11** or paclitaxel are compared to controls. The comparison of tumor volumes between control and drug-treated groups on day 9 is indicated. Mice were treated on days 1, 3, and 5 with either 75 mg/kg of **11** or 10 mg/kg of

paclitaxel, and the trial was halted on day 9 due to the large size of tumors in control and paclitaxel-treated mice. n = 8-9 tumors per group.

5. Summary

A series of nine novel N5-substituted-pyrrolo[3,2-*d*]pyrimidin-4-amines were designed, synthesized and evaluated as MTAs. Several of these analogs were significantly more potent than the lead compounds. Each of the potent novel compounds were able to circumvent drug resistance mediated by Pgp and βIII-tubulin. ^{1}H NMR and molecular modeling of the most active compounds indicate a syn conformation of the N4-aryl substitution with respect to the scaffold. Compound **11**, freely water soluble as the corresponding HCl salt, demonstrated statistically significant antitumor effects in three in vivo xenograft models (MDA-MB-435, MDA-MB-231 and NCI/ADR-RES) with antitumor activity superior to that of paclitaxel in the NCI/ADR-RES tumor model. Compound **11** will be further evaluated in preclinical studies for consideration for advancement into clinical trials.

6. Experimental section

6.1 Synthesis

4-Chloro-2,5-dimethyl-5*H*-pyrrolo[3,2-*d*]pyrimidine (15)

4-Chloro-2-methyl-5*H*-pyrrolo[3,2-*d*]pyrimidine (**14**,[8] 300 mg, 1.79 mmol) was dissolved in dimethylformamide (20 mL), and sodium hydride (47 mg, 1.97 mmol) was added under nitrogen. The mixture was stirred for 15 min, when no further production of hydrogen gas was observed. Methyl bromide (0.3 mL) was added, and the reaction mixture was stirred for 3 h. The reaction was quenched by addition of water, and ethyl acetate was added. The organic layer was collected, washed with brine and dried over sodium sulfate. A silica gel plug was made, and **15**

was purified by column chromatography ($CHCl_3$: MeOH; 100:1 v/v) as an off-white solid (244 mg, 75%). TLC R_f = 0.45 (CH_3OH: $CHCl_3$; 1:10); mp, 156-158 °C; ^1H NMR (400 MHz, DMSO-d_6) δ = 2.62 (s, 3 H, CH_3) 4.01 (s, 3 H, CH_3) 6.6 (m, 1 H, 7-CH) 7.9 (m, 1 H, 6-CH).

_N_-(4-Methoxyphenyl)-_N_,2,5-trimethyl-5_H_-pyrrolo[3,2-_d_]pyrimidin-4-amine hydrochloride (5·HCl)

Compound **5**·HCl (synthesized from **15** and 4-methoxy *N*-methyl aniline as described previously[8]): yield 76%; TLC R_f = 0.55 (CH_3OH: $CHCl_3$; 1:10); white solid; mp, 218-220 °C; ^1H NMR (400 MHz, DMSO-d_6) δ = 2.69 (s, 3 H, CH_3) 2.84 (s, 3 H, CH_3) 3.63 (s, 3 H, CH_3) 3.79 (s, 3 H, CH_3) 6.51 (d, J = 3.26 Hz, 1 H, Ar) 7.00 - 7.03 (m, 2 H, Ar) 7.27 - 7.31 (m, 2 H, Ar) 7.65 (d, J = 3.26 Hz, 1 H, Ar) 15.11 (s, 1 H, exch, HCl) Anal. Calcd. for $C_{16}H_{18}N_4O$·HCl: C, 60.28; H, 6.01; N, 17.57; Cl, 11.12. Found C, 60.52; H, 5.97; N, 17.53; Cl, 10.88.

_N_-(4-methoxyphenyl)-2,5-dimethyl-5_H_-pyrrolo[3,2-_d_]pyrimidin-4-amine hydrochloride (6·HCl)

Compound **6**·HCl (synthesized from **15** and *p*-anisidine as described previously[8]): yield 81%; TLC R_f = 0.48 (CH_3OH: $CHCl_3$; 1:10); white solid; mp, 317-319 °C; ^1H NMR (400 MHz, DMSO-d_6) δ = 2.50 (s, 3 H, CH_3) 3.80 (s, 3 H, CH_3) 4.23 (s, 3 H, CH_3) 6.50 (d, J = 3.01 Hz, 1 H, Ar) 7.00 - 7.04 (m, 2 H, Ar) 7.47 - 7.51 (m, 2 H, Ar) 7.83 (d, J = 3.01 Hz, 1 H, Ar) 9.52 (s, 1 H, exch, NH) 14.70 (br, 1 H, exch, HCl) Anal. Calcd. for $C_{15}H_{16}N_4O$·HCl: C, 59.11; H, 5.62; N, 18.38; Cl, 11.63. Found C, 59.32; H, 5.68; N, 18.36; Cl, 11.37.

_N_-(2,4-dimethoxyphenyl)-2,5-dimethyl-5_H_-pyrrolo[3,2-_d_]pyrimidin-4-amine hydrochloride (7·HCl)

Compound **7**·HCl (synthesized from **15** and 2,4-dimethoxy aniline as described previously[8]): yield 77%; TLC R_f = 0.4 (CH_3OH: $CHCl_3$; 1:10); white solid; mp, 246-248 °C; ^1H NMR (400 MHz, DMSO-d_6) δ 2.5 (s, 3 H, CH_3) 2.84 (s, 3 H, CH_3) 3.80 (s, 3 H), 4.23 (s, 3 H), 6.50 (d, J= 3.0 Hz, 1 H), 7.02 (s, 1 H, Ar), 7.47 – 7.52 (m, 2 H, Ar), 7.83 (s, 1 H, Ar), 9.52 (s, 1 H, exch, NH), 14.68 (s, 1 H, exch, NH). Anal. Calcd. for $C_{16}H_{18}N_4O_2$·HCl: C, 57.40; H, 5.72; N, 16.73; Cl, 10.59. Found C, 57.31; H, 5.80; N, 16.56; Cl, 10.37.

1-(2,5-dimethyl-5_H_-pyrrolo[3,2-_d_]pyrimidin-4-yl)-6-methoxy-1,2,3,4-tetrahydroquinoline hydrochloride (8·HCl)

Compound **8**·HCl (synthesized from **15** and 6-methoxy-1,2,3,4-tetrahydroquinoline as described previously[8]): yield 77%; TLC R_f = 0.5 (CH_3OH: $CHCl_3$; 1:10); yellow solid; mp, 230-232 °C; ^1H NMR (400 MHz, DMSO-d_6) δ = 2.08 (quin, J = 6.59 Hz, 2 H, CH_2) 2.67 (s, 3 H, CH_3) 2.86 (t, J = 6.53 Hz, 2 H, CH_2) 3.00 (s, 3 H, CH_3) 3.76 (s, 3 H, CH_3) 4.03 (t, J = 6.02 Hz, 2 H, CH_2) 6.56 (d, J = 3.01 Hz, 1 H, Ar) 6.69 - 6.72 (m, 1 H, Ar) 6.76 - 6.79 (m, 1 H, Ar) 6.94 (d, J = 2.76 Hz, 1 H, Ar) 7.74 (d, J = 3.01 Hz, 1 H, Ar) 14.97 (b, 1 H, exch, HCl) Anal. Calcd. for $C_{18}H_{20}N_4O$·HCl: C, 62.69; H, 6.14; N, 16.25; Cl, 10.28. Found C, 62.62; H, 6.09; N, 6.10; Cl, 10.10.

5-ethyl-_N_-(4-methoxyphenyl)-_N_,2-dimethyl-5_H_-pyrrolo[3,2-_d_]pyrimidin-4-amine (9)

_N_-(4-methoxyphenyl)-_N_,2-dimethyl-5_H_-pyrrolo[3,2-_d_]pyrimidin-4-amine (**1**, 100 mg, 0.373 mmol) was dissolved in dimethylformamide (6 mL), and sodium hydride (10.73 mg, 0.447 mmol) was added under nitrogen. The mixture was stirred for 15 min, when no further production of hydrogen gas was observed. Ethyl iodide (0.1 mL) was added, and the reaction

mixture was stirred for 3 h. The reaction was quenched by addition of water and ethyl acetate was added. The organic layer was collected, washed with brine and dried over sodium sulfate. A silica gel plug was made, and **9** was purified by column chromatography ($CHCl_3$: CH_3OH; 100:1 v/v) as an off-white solid (726 mg, 75%). TLC R_f = 0.42 (CH_3OH: $CHCl_3$; 1:20); mp, 145-147 °C; ^1H NMR (400 MHz, DMSO-d_6) δ = 1.30 - 1.42 (m, 3 H, CH_3) 2.69 (s, 3 H, CH_3) 2.87 (q, J = 7.15 Hz, 2 H, CH_2) 3.64 (s, 3 H, CH_3) 3.79 (s, 3 H, CH_3) 6.54 (d, J = 3.26 Hz, 1 H, Ar) 7.01 (d, J = 9.03 Hz, 2 H, Ar) 7.29 (d, J = 9.03 Hz, 2 H, Ar) 7.75 (d, J = 3.26 Hz, 1 H, Ar) Anal. Calcd. for $C_{17}H_{20}N_4O$: C, 68.89; H, 6.80; N, 18.90. Found C, 68.78; H, 6.05; N, 18.59.

5-isopropyl-*N*-(4-methoxyphenyl)-*N*,2-dimethyl-5*H*-pyrrolo[3,2-*d*]pyrimidin-4-amine hydrochloride (10·HCl)

Compound **10**·HCl (synthesized from **1** and *iso*-propyl bromide as described for **9**): yield = 78%; TLC R_f = 0.51 (CH_3OH: $CHCl_3$; 1:20); grey solid; mp, 244-246 °C; ^1H NMR (400 MHz, DMSO-d_6) δ 0.85 (d, J = 6.3 Hz, 6 H, CH_3), 2.72 (s, 3 H, CH_3), 3.61 (s, 3 H, CH_3), 3.76 (s, 3 H, CH_3), 4.07 (p, J = 6.8 Hz, 1 H, CH), 6.64 – 6.68 (m, 1 H, Ar), 6.94 – 7.01 (m, 2 H, Ar), 7.18 (s, 2 H, Ar), 7.98 (d, J = 3.4 Hz, 1 H, Ar), 15.25 (br, 1 H, exch, NH). Anal. Calcd. for $C_{18}H_{22}N_4O$·HCl: C, 62.33; H, 6.68; N, 16.15; Cl, 10.22. Found C, 62.19; H, 6.69; N, 16.00; Cl, 10.13.

***N*-(4-methoxyphenyl)-*N*,2-dimethyl-5-propyl-5*H*-pyrrolo[3,2-*d*]pyrimidin-4-amine hydrochloride (11·HCl)**

Compound **11**·HCl (synthesized from **1** and *n*-propyl bromide as described for **9**): yield = 83%; TLC R_f = 0.5 (CH_3OH: $CHCl_3$; 1:20); light yellow solid; mp, 214-216 °C; ^1H NMR (400 MHz,

DMSO-d_6) δ = 0.47 (t, J = 7.28 Hz, 3 H, CH_3) 1.30 - 1.42 (m, 2 H, CH_2) 2.69 (s, 3 H, CH_3) 2.87 (t, J = 7.15 Hz, 2 H, CH_2) 3.64 (s, 3 H, CH_3) 3.79 (s, 3 H, CH_3) 6.54 (d, J = 3.26 Hz, 1 H, Ar) 7.01 (d, J = 9.03 Hz, 2 H, Ar) 7.29 (d, J = 9.03 Hz, 2 H, Ar) 7.75 (d, J = 3.26 Hz, 1 H, Ar) 15.11 (br, 1 H, exch, NH). Anal. Calcd. for $C_{18}H_{22}N_4O$·HCl: C, 62.33; H, 6.68; N, 16.15; Cl, 10.22. Found C, 62.17; H, 6.70; N, 15.98; Cl, 10.12.

5-isobutyl-*N*-(4-methoxyphenyl)-*N*,2-dimethyl-5*H*-pyrrolo[3,2-*d*]pyrimidin-4-amine hydrochloride (12·HCl)

Compound **12**·HCl (synthesized from **1** and *iso*-butyl bromide as described for **9**): yield = 80%; TLC R_f = 0.55 (CH_3OH: $CHCl_3$; 1:20); white solid; mp, 260-261 °C; ^{1}H NMR (400 MHz, DMSO-d_6) δ = 0.59 (J = 6.3 Hz, 6 H, CH_3) 1.02 - 1.14 (m, 1 H, CH) 2.70 (s, 3 H, CH_3) 2.90 (m, 2 H, CH_2) 3.63 (s, 3 H, CH_3) 3.78 (s, 3 H, CH_3) 6.58 (d, J = 3.1 Hz, 1 H, Ar) 7.00 (d, J = 9 Hz, 2 H, Ar) 7.25 (d, J = 9 Hz, 2 H, Ar) 7.83 (d, J = 3.15 Hz, 1 H, Ar) 15.13 (br, 1 H, exch, NH). Anal. Calcd. for $C_{19}H_{24}N_4O$·HCl: C, 63.23; H, 6.98; N, 15.52; Cl, 9.82. Found C, 63.20; H, 7.01; N, 15.39; Cl, 9.65.

5-butyl-*N*-(4-methoxyphenyl)-*N*,2-dimethyl-5*H*-pyrrolo[3,2-*d*]pyrimidin-4-amine hydrochloride (13·HCl)

Compound **13**·HCl (synthesized from **1** and *n*-butyl bromide as described for **9**): yield = 77%; TLC R_f =0.6 (CH_3OH: $CHCl_3$; 1:20); white solid; mp, 229-230 °C; ^{1}H NMR (400 MHz, DMSO-d_6) δ = 0.69 - 0.75 (m, 3 H, CH_3) 0.76 - 0.85 (m, 2 H, CH_2) 1.25 - 1.34 (m, 2 H, CH_2) 2.69 (s, 3 H, CH_3) 2.94 (t, J = 7.15 Hz, 2 H, CH_2) 3.65 (s, 3 H, CH_3) 3.79 (s, 3 H, CH_3) 6.54 (d, J = 3.26 Hz, 1 H, Ar) 7.01 (d, J = 9.03 Hz, 2 H, Ar) 7.28 (d, J = 9.03 Hz, 2 H, Ar) 7.76 (d, J = 3.26 Hz, 1

H, Ar) 15.03 (br, 1 H, exch, NH). Anal. Calcd. for $C_{19}H_{24}N_4O \cdot HCl$: C, 63.24; H, 6.98; N, 15.52; Cl, 9.82. Found C, 63.29; H, 6.91; N, 15.50; Cl, 9.66.

6.2 Molecular modeling

Docking of compounds **2-13** was carried out in the published X-ray crystal structure of colchicine in tubulin (PDB: 4O2B, 2.3 Å)[12] using Schrödinger.[13] The ligands were sketched in Schrödinger, minimized in energy, and prepared using the LigPrep module, using the default parameters. The crystal structure of tubulin was obtained from the protein database and prepared using the default parameters, using the protein preparation wizard. The receptor grid was generated using colchicine as the reference ligand. The docking was carried out with the GLIDE module with XP (extra precision), flexible ligand sampling and with an output maximum of 5 poses per ligand. The docking method was validated by performing re-docking of the native ligand colchicine. Superimposition of the best docked pose of colchicine in tubulin was exactly the same as the co-crystallized ligand.

6.3 Cell culture

A-10 embryonic rat aortic smooth muscle, HeLa cervical carcinoma, SK-OV-3 ovarian carcinoma, and MDA-MB-231 breast carcinoma cell lines were obtained directly from ATCC (Manassas, VA). The MDA-MB-435 melanoma cells were acquired from the Lombardi Cancer Center (Georgetown University) and validated by ATCC. NCI/ADR-RES cells were obtained from the NIH (Bethesda, MD). The SK-OV-3/MDR-1-6/6 and HeLa wild-type βIII (WT βIII) cell lines were described previously.[17] MDA-MB-435, MDA-MB-231 and NCI/ADR-RES cells were cultured in Improved Minimum Essential Medium (Richter's Modification) (Gibco, Life Technologies, Grand Island, NY) with 10% fetal bovine serum and 25 µg/mL gentamicin. WT

βIII cells were grown in DMEM (Gibco, Life Technologies) with 10% fetal bovine serum and 50 µg/mL gentamicin, while all the other cell lines were maintained in Basal Medium Eagle (Sigma-Aldrich) with 10% fetal bovine serum and 50 µg/mL gentamicin. All cells were maintained in a humidified incubator at 37 °C with 5% CO_2.

6.3.1 Microtubule depolymerization assay

The effects of the compounds on cellular microtubules were evaluated by indirect immunofluorescence techniques as described in detail previously.[18, 19] Briefly, A-10 cells were plated onto glass coverslips, allowed to attach and grow and then treated for 18 h with compounds. Paclitaxel and CA-4 were used as positive controls and vehicle (DMSO) as a negative control. Cells were fixed and microtubules visualized with a β-tubulin antibody and DNA visualized with DAPI. The effects of the compounds on interphase microtubules were evaluated using a Nikon Eclipse Ti80 microscope. The effects of a range of concentrations of each compound were evaluated, and percent microtubule loss was estimated visually for each treatment. The EC_{50}, the concentration that caused 50% microtubule depolymerization, was calculated from concentration response curves generated from at least 3 independent experiments as described previously.[18, 19]

6.3.2 Sulforhodamine B (SRB) Assay

The ability of the compounds to inhibit cellular proliferation was evaluated using the sulforhodamine B (SRB) assay as previously described.[17] In brief, cells were plated at predetermined densities into 96-well plates, allowed to attach and proliferate for 24 h, and then

the compounds or vehicle control (DMSO) were added to triplicate wells. Cells were exposed to a range of compound concentrations for 48 h, fixed and cellular protein stained with SRB. The IC_{50} values were calculated from the linear portions of the log-concentration response curves of at least three independent experiments. The IC_{50} values are expressed as mean ± SD.

6.3.3 In vivo antitumor effects

Athymic nude (*Foxn1*^{nu}/*Foxn1*^{nu}) female mice (6 weeks old) were purchased from Harlan Laboratories (Indianapolis, IN). Tumor fragments were implanted bilaterally on each flank for the MDA-MB-435 trial. When tumors reached approximately 200 mm^3, mice were placed into groups of five (10 tumors per group) to provide similar tumor volume per group, and then the groups were randomly assigned a treatment. Compound **5** was solubilized in ethanol and **11** in H_2O to a concentration of 200 mg/mL, and then each was diluted into PBS such that solvent concentration was less than 5% just before injections in a total volume of ~0.2 mL. Compounds **5** and **11** were administered using i.p. injections at a dose of 75 mg/kg. Compound **5** was administered on days 1, 2, 3, 4 and 9 for a cumulative dose of 375 mg/kg. Compound **11** was dosed on days 1, 2, 3, 4, 7, 9 and 11 for a cumulative dose of 525 mg/kg. Tumors were measured with calipers to obtain width x length x height to yield tumor volume (mm^3), and tumor mass (g) was determined by weighting the tumors that were removed at the end of the trial. Individual mouse weights were monitored over the duration of the trial as a sign of toxicity.

The MDA-MB-231 in vivo trial was conducted as described above except MDA-MB-231 tumor fragments were implanted into the flank bilaterally and groups consisted of 7-10 tumors. The treatment groups consisted of untreated controls, **11** at 75/mg/kg and paclitaxel at 10 mg/kg. The mice were dosed on days 1, 2, 3, 8, 9 and 10. **11** was formulated and administered as

described above, and paclitaxel was suspended 50:50 in ethanol:Cremophor to a concentration of 20 mg/mL and then diluted into PBS for a final solvent concentration < 7%.

In the NCI/ADR trial, NCI/ADR-RES tumors were transplanted bilaterally into mouse flanks and the trails conducted as described above, except the mice were treated with **11** or paclitaxel with the doses described above on days 1, 3 and 5 with 8-9 tumors per group. This trial was ended on day 9 due to the size of some of the tumors in the control and paclitaxel-treated groups.

The in vivo studies were conducted in accordance with the NIH guidelines as described in the Guide for the Care and Use of Laboratory Animals, and the protocols were approved by the UT Health Institutional Animal Care and Use Committee. Mice were housed in an AALAC approved facility, and food and water were provided *ad libitum*.

Acknowledgements

We gratefully acknowledge the NCI for performing the in vitro antitumor evaluation in their 60 cancer cell line panel. This work was supported, in part, by the National Institutes of Health and NCI grants RO1 CA142868 (AG, SLM), a NSF equipment grant for NMR instrumentation (NMR: CHE 0614785) and the Duquesne University Adrian Van Kaam Chair in Scholarly Excellence (A.G.). Educational support for Nicholas Dybdal-Hargreaves was provided by the COSTAR training grant (T32-DE014318).

References

1. Hanahan, D.; Weinberg, R. A. *Cell* **2011**, *144*, 646-674.

2. Hall, A. *Cancer Metastasis Rev.* **2009**, *28*, 5-14.

3. Ogden, A.; Rida, P. C.; Reid, M. D.; Aneja, R. *Drug Discov. Today* **2014**, *19*, 824-829.

4. Komlodi-Pasztor, E.; Sackett, D. L.; Fojo, A. T. *Clin. Cancer Res.* **2012**, *18*, 51-63.

5. Jordan, M. A.; Kamath, K. *Curr. Cancer Drug Targets* **2007**, *7*, 730-742.

6. Wang, Z.; Sun, Y. *Transl. Oncol.* **2010**, *3*, 1-12.

7. O'Connor, P. M.; Jackman, J.; Bae, I.; Myers, T. G.; Fan, S.; Mutoh, M.; Scudiero, D. A.; Monks, A.; Sausville, E. A.; Weinstein, J. N.; Friend, S.; Fornace, A. J., Jr.; Kohn, K. W. *Cancer Res.* **1997**, *57*, 4285-4300.

8. Gangjee, A.; Pavana, R. K.; Li, W.; Hamel, E.; Westbrook, C.; Mooberry, S. L. *Pharm. Res.* **2012**, *29*, 3033-3039.

9. SYBYL-X 2.1.1, Tripos International, 1699 South Hanley Rd., St. Louis, Missouri, 63144, USA.

10. Gangjee, A.; Pavana, R. K.; Ihnat, M. A.; Thorpe, J. E.; Disch, B. C.; Bastian, A.; Bailey-Downs, L. C.; Hamel, E.; Bai, R. *ACS Med. Chem. Lett.* **2014**, *5*, 480-484.

11. Pavana, R. K.; Choudhary, S.; Bastian, A.; Ihnat, M. A.; Bai, R.; Hamel, E.; Gangjee, A. *Bioorg. Med. Chem.* **2017**, *25*, 545-556.

12. Prota, A. E.; Danel, F.; Bachmann, F.; Bargsten, K.; Buey, R. M.; Pohlmann, J.; Reinelt, S.; Lane, H.; Steinmetz, M. O. *J. Mol. Biol.* **2014**, *426*, 1848-1860.

13. Small-Molecule Drug Discovery Suite 2018-1, Schrödinger, LLC, New York, NY, 2018.

14. Banerjee, S.; Arnst, K. E.; Wang, Y.; Kumar, G.; Deng, S.; Yang, L.; Li, G. B..; Yang, J.; White, S. W.; Li, W.; Miller, D. D. *J. Med. Chem.* **2018**, *61*, 1704-1718.

15. Devambatla, R. K. V.; Namjoshi, O. A.; Choudhary, S.; Hamel, E.; Shaffer, C. V.; Rohena, C. C.; Mooberry, S. L.; Gangjee, A. *J. Med. Chem.* **2016**, *59*, 5752-5765.

16. Tron, G. C.; Pirali, T.; Sorba, G.; Pagliai, F.; Busacca, S.; Genazzani, A. A. *J. Med. Chem.* **2006**, *49*, 3033-3044.

17. Risinger, A. L.; Jackson, E. M.; Polin, L. A.; Helms, G. L.; LeBoeuf, D. A.; Joe, P. A.; Hopper-Borge, E.; Luduena, R. F.; Kruh, G. D.; Mooberry, S. L. *Cancer Res.* **2008**, *68*, 8881-8888.

18. Gangjee, A.; Zhao, Y.; Lin, L.; Raghavan, S.; Roberts, E. G.; Risinger, A. L.; Hamel, E.; Mooberry, S. L. *J. Med. Chem.* **2010**, *53*, 8116-8128.

19. Lee, L.; Robb, L. M.; Lee, M.; Davis, R.; Mackay, H.; Chavda, S.; Babu, B.; O'Brien, E. L.; Risinger, A. L.; Mooberry, S. L.; Lee, M. *J. Med. Chem.* **2010**, *53*, 325-334.

1 **5**

	IC_{50} (nM) MDA-MB-435	**EC_{50} (nM) microtubule depolymerization**
1	96	1200
5	4.3	7.4